# Using optimal control to obtain maximum displacement gait for Purcell's three-link swimmer

Oren Wiezel and Yizhar Or

***Abstract*— Purcell's swimmer is a classical model of a simple three-link swimmer moving in a highly viscous fluid, similar to the motion of microscopic organisms or robotic microswimmers. The two joint angles are commonly prescribed as periodic trajectories called gaits, so that the dynamics of Purcell's swimmer can be formulated as a driftless nonlinear control system. In a famous paper by Tam and Hosoi, they have found the optimal gait that maximizes net displacement over a cycle by representing the time-periodic joint angles as truncated Fourier series and numerically optimizing a finite set of their coefficients. In this work, the gait optimization is revisited and analytically formulated as an elegant problem of optimal control system with only two state variables and a single input, which can be solved using Pontryagin's maximum principle. Due to absence of any physical constraints on the control system's input, it turns out that the optimal solution must follow a "singular arc". Numerical solution of the boundary value problem is obtained, which exactly reproduces Tam and Hosoi's optimal gait.**

## I. INTRODUCTION

The dynamics of swimming in a viscous fluid has recently become a subject of extensive research, focusing particularly on micron-size swimmers. Scientists are striving to understand the behavior of swimming microorganisms such as bacteria and sperm cells [1], [2]. Engineers are developing micro-robotic swimmers propelled using several actuation methods [3], [4], which are aimed towards future biomedical applications inside the human body such as targeted drug delivery and minimally invasive surgery [5], [6], [7]. An important aspect of this research area is analysis of simple mechanical models of microswimmers from the perspective of dynamical systems and control theory [8], [9].

The dynamics of micron-size swimmers is governed by low Reynolds number hydrodynamics where viscous drag effects dominate while inertial effects are negligible. In this regime, drag forces are linearly related to velocities, a fact that enables formulation of the swimmer's dynamics as a driftless nonlinear control system [10]. It is commonly assumed that the swimmer's shape parameters are directly controlled and vary along time-periodic trajectories called *gaits*. Microswimmers can thus be classified as principal locomotion systems, which have been extensively analyzed in the literature of robotics and control, using notions such as geometric mechanics and Lie groups for studying nonlinear controllability [11] and gait planning [12], [13]. Interestingly, large swimmers, whose motion is governed by inertial effects and are commonly modelled under the assumption of "inviscid fluid", also belong to the same class of locomotion systems, and are analyzed using similar techniques [14], [15].

Purcell's classical model of a three-link planar microswimmer has been introduced in 1977 in [16], see Fig. 1a. It consists of three elongated rigid links connected by two revolute joints whose angles $\phi_1$ and $\phi_2$ vary in time along a prescribed periodic gait. Purcell proposed a simple "square gait" where the two joints are rotating alternately (Fig. 1b) and stated, using symmetry considerations, that the net motion over one cycle is translation along the middle link's longitudinal axis. Only 26 year later, Becker *et al* [17] have obtained an explicit formulation of the dynamics of Purcell's three-link swimmer by using resistive force theory (RFT) to formulate the viscous drag forces assuming slender links [18], [19]. Symmetries and gaits of Purcell's swimmer have been studied in [20], [21], and geometric methods for gait planning have been proposed in [15]. Results of motion experiments of macro-scale robotic versions of Purcell's swimmer in a viscous fluid have been reported in [21], [22], [23], where the controlled gaits were mostly limited to simple alternating motion of the joints. The recent work [24] has studied optimal stroke amplitudes of Purcell's swimmer for maximal displacement or energetic efficiency under the square gait, as well as a circular gait where the two joint angles oscillate sinusoidally in a quarter-period phase shift.

An important theoretical result has been presented in 2007 by Tam and Hosoi [25], who found an optimal gait of joint angles which maximizes the net displacement for Purcell's swimmer, see Fig. 1c. This gait has been obtained by representing the time-periodic joint angles $\phi_i(t)$ as truncated Fourier series and conducting numerical optimization on the finite set of series coefficients. A similar approach has been applied for optimizing energetic efficiency of one-dimensional motion of axisymmetric microswimmers under small deformations [26] and large strokes [27], as well as an actuated elastic flagellum in [28]. This method typically requires extensive computational effort, and may be highly sensitive to initial guess and get trapped in solutions of local optimum.

An alternative approach is using the classical technique of *optimal control* [29], [30], and particularly Potryagin's maximum principle [31], which is based on calculus of variations. This technique has been applied to robotic locomotion systems in [32], and even to a discrete mechanics optimal control scheme [33], [34], [35]. In low-Reynolds number swimming, [36] has used optimal control to find energy-efficient gaits for the one-dimensional motion of an axisymmetric swimmer, and [37] employed a computational

O. Wiezel and Y. Or are with the Faculty of Mechanical Engineering, Technion - Israel Institute of Technology, Haifa 32000, Israel izi@technion.ac.il

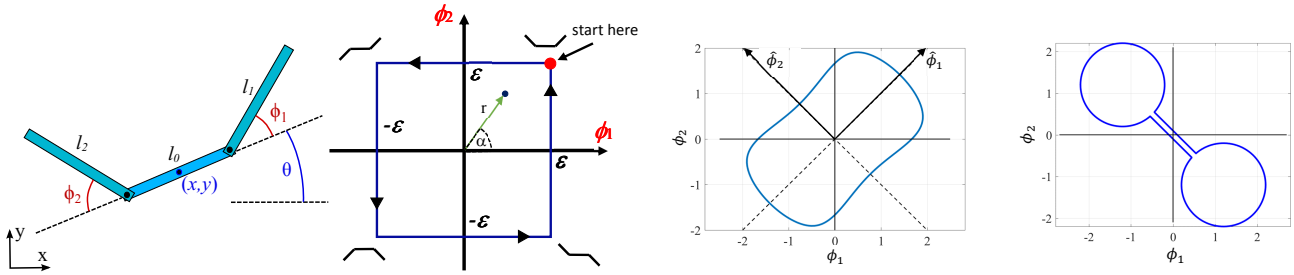


Fig. 1: (a) Purcell's 3-link swimmer. (b) The square gait. (c) Tam & Hosoi's optimal gait. (d) The dumbbell gait.

optimal control tool to study energy-efficient gaits for planar motion of multi-link microswimmers. In [38], optimal gaits for maximal displacement of Purcell's swimmer are obtained by formulating a constrained optimal control problem with bounds on the joints angles and angular velocities. The resulting gaits are polygonal loops in $(\phi_1, \phi_2)$ plane which follow "bang-bang" solutions where one of the bounds is reached for a finite time. These gaits are all sub-optimal with respect to the smooth curve of optimal gait obtained by Tam and Hosoi (Fig. 1d), which seems not to be bounded by any constraints on angles and especially not velocities, since the net displacement is invariant with respect to time-parametrization of the motion along the gait's trajectory.

Interestingly, one constraint that Tam and Hosoi [25] implicitly assumed is that the gait should be a symmetric "simple loop". In a follow-up comment by Raz and Avron [39], they proposed a dumbbell-shaped gait as illustrated in Fig. 1d and showed that it outperforms the displacement achieved by the optimal gait in [25]. In their response, Tam and Hosoi classified the dumbbell gait as a "composite gait made of multiple almost-closed loops", and argued informally that the analysis should focus on gaits of simple loops while composite gaits should be discarded.

The goal of this work is to revisit this problem and formulate it as an optimal control problem without constraints. In order to avoid gaits of composite loops, we represent the gait in polar coordinates $(r, \alpha)$ as shown in Fig. 1b, such that the gait is described by a single smooth function $r(\alpha)$ that represents a simple loop. Using RFT approximation, we then formulate the system's dynamics in only two state variables and a single input, and define a cost function of net displacement $X$ to be maximized. The system's Hamiltonian $H$ depends linearly on the control input $u(t)$, a fact that commonly lead to a "bang-bang" solution. Due to absence of any physical bounds or constraints on the trajectory, the optimal solution follows a *singular arc* [29], [30] where $dH/du = 0$ for all $t$. After a reduction, a boundary value problem of three nonlinear differential equations is obtained and solved numerically, and its solution exactly reproduces Tam and Hosoi's optimal gait. Finally, the computation is utilized for numerically obtaining optimal ratio of the swimmer's links lengths that achieves maximal displacement.

## II. Formulation of Purcell's Swimmer Dynamics

In this section we introduce Purcell's swimmer and formulate its dynamic equations of motion. The swimmer model consists of three thin rigid links with lengths $l_0, l_1, l_2$, where $l_1 = l_2$ . The links are connected by two rotary joints whose angles are denoted by $\phi_1$ and $\phi_2$ (see Fig. 1a). The shape of the swimmer is denoted by the vector $\boldsymbol{\phi} = (\phi_1, \phi_2)^T$. It is assumed that the swimmer's motion is confined to a plane. The planar position of the middle link's center is $(x, y)$ and its orientation angle is $\theta$. The swimmer is submerged in an unbounded fluid domain whose motion is governed by Stokes equations [40]. The velocity of the $i$th link is described by the linear velocity of its center $\mathbf{v}_i$ and the links angular velocity $\omega_i$ , which are augmented in the vector $\mathbf{V}_i = (\mathbf{v}_i, \omega_i) \in \mathbb{R}^3$. Similarly, define the body velocity vector as $\mathbf{V}_b = (\dot{x}, \dot{y}, \dot{\theta})^T$, which denotes the linear and angular velocities of a reference frame attached to the central link.

The kinematic relation between the body velocity $\mathbf{V}_b$, the joints velocities $\dot{\boldsymbol{\phi}}$ and the links velocities $\mathbf{V}_i$ can be written in matrix form:

$$\mathbf{V}_i = \mathbf{T}_i(\theta, \boldsymbol{\phi})\mathbf{V}_b + \mathbf{E}_i(\theta, \boldsymbol{\phi})\dot{\boldsymbol{\phi}}. \tag{1}$$

The matrices $\mathbf{T}_i(\theta, \boldsymbol{\phi})$ and $\mathbf{E}_i(\theta, \boldsymbol{\phi})$ for $i = 0, 1, 2$ are given by:

$$\begin{aligned}
\mathbf{T}_0 &= \begin{bmatrix} 1 & 0 & 0 \\ 0 & 1 & 0 \\ 0 & 0 & 1 \end{bmatrix}, \ \mathbf{E}_0 = \begin{bmatrix} 0 & 0 \\ 0 & 0 \\ 0 & 0 \end{bmatrix} \\
\mathbf{T}_1 &= \begin{bmatrix} 1 & 0 & +0.5l_o \sin\alpha_0 - 0.5l_1 \sin\alpha_1 \\ 0 & 1 & -0.5l_0 \cos\alpha_0 - 0.5l_1 \cos\alpha_1 \\ 0 & 0 & 1 \end{bmatrix}, \mathbf{E}_1 = \begin{bmatrix} 0.5l_1 \sin\alpha_1 & 0 \\ 0.5l_1 \cos\alpha_1 & 0 \\ -1 & 0 \end{bmatrix} \\
\mathbf{T}_2 &= \begin{bmatrix} 1 & 0 & -0.5l_o \sin\alpha_o - 0.5l_2 \sin\alpha_2 \\ 0 & 1 & 0.5l_o \cos\alpha_o + 0.5l_2 \cos\alpha_2 \\ 0 & 0 & 1 \end{bmatrix}, \mathbf{E}_2 = \begin{bmatrix} 0 & -0.5l_2 \sin\alpha_2 \\ 0 & 0.5l_2 \cos\alpha_2 \\ 0 & 1 \end{bmatrix},
\end{aligned} \tag{2}$$

Where $\alpha_0 = \theta$ ,$\alpha_1 = \phi_1 - \theta$ , and $\alpha_2 = \theta + \phi_2$ are the absolute rotation angles of each link. Next, we apply resistive force theory [18], which states that the viscous drag force $\mathbf{f}_i$ and torque $m_i$ on the $i$th slender link under planar motion are proportional to its linear and angular velocities. Thus, we can write the expression for the force exerted on each link:

$$\begin{aligned}
\mathbf{f}_i &= -c_t l_i (\mathbf{v}_i \cdot \mathbf{t}_i)\mathbf{t}_i - c_n l_i (\mathbf{v}_i \cdot \mathbf{n}_i)\mathbf{n}_i \\
m_i &= -\frac{1}{12} c_n l_i^3 \omega_i,
\end{aligned} \tag{3}$$

Where $\mathbf{t}_i = (\cos\alpha_i, \sin\alpha_i)^T$ is a unit vector in the axial direction of the $i$th link and $\mathbf{n}_i = (-\sin\alpha_i, \cos\alpha_i)^T$ is a unit vector in the normal direction. The resistance coefficients for the normal and axial directions are $c_n = 2\mathrm{c_t} = 4\pi\mu/log(l_c/a)$, where $\mu$ is the dynamic viscosity of the fluid, $a$ is the radius of the links' cross-section and $l_c$ is a characteristic length. It is assumed that the hydrodynamic interaction between the links is negligible. Denoting the vector of forces and torques on the $i$th link as $\mathbf{F}_i = (\mathbf{f}_i, m_i)$ the relation (3) can be written in matrix form

$$\mathbf{F}_i = -\mathcal{R}_i(\theta, \boldsymbol{\phi})\mathbf{V}_i \tag{4}$$

where:

$$\mathcal{R}_i(\theta, \boldsymbol{\phi}) = \mathrm{c_t}^{(i)} l_i \begin{bmatrix} 1+\sin^2\alpha_i & -\cos\alpha_i\sin\alpha_i & 0 \\ -\cos\alpha_i\sin\alpha_i & 1+\cos^2\alpha_i & 0 \\ 0 & 0 & \frac{1}{6}l_i^2 \end{bmatrix} \tag{5}$$

is called the resistance tensor. Using the kinematic relation (1), the net hydrodynamic force and torque acting on the swimmer's body frame, $\mathbf{F}_b$, are given by:

$$\mathbf{F}_b = \sum_{i=0}^{2} \mathbf{T}_i^T \mathbf{F}_i = -\sum_{i=0}^{2} \mathbf{T}_i^T \boldsymbol{\mathcal{R}}_i(\mathbf{T}_i\mathbf{V}_b + \mathbf{E}_i\dot{\boldsymbol{\phi}}). \tag{6}$$

Assuming quasi-static motion, the swimmer is in static equilibrium $\mathbf{F}_b = 0$. Substituting into (6), the swimmer's dynamic equation of motion is obtained as:

$$\mathbf{V}_b = \mathbf{G}(\theta, \boldsymbol{\phi})\dot{\boldsymbol{\phi}} \tag{7}$$

Where:

$$\mathbf{G}(\theta, \boldsymbol{\phi}) = -\left(\sum_{i=0}^{2} \mathbf{T}_i^T \mathcal{R}_i \mathbf{T}_i\right)^{-1} \left(\sum_{i=0}^{2} \mathbf{T}_i^T \mathcal{R}_i \mathbf{E}_i\right) \tag{8}$$

Note that since there are no external boundary conditions in the unbounded fluid domain, the angular velocity of the swimmer $\dot{\theta}$ in (7) is independent of $\theta$. Some additional symmetry properties of $\mathbf{G}$ in (8) have been found in previous research [21]. Specifically, it has been proven that a gait which is symmetric with respect to the two diagonal lines $\phi_1 = \phi_2$ and $\phi_1 = -\phi_2$ (Fig. 1c) and starts on $\phi_1 = \phi_2$ results in net displacement only in the longitudinal $x$ direction of the middle link at its initial state, with no net displacement in the perpendicular direction or net rotation of the swimmer. The total displacement in the $x$ direction over one cycle will be denoted by $X$.

## III. Finding Optimal Gaits

In this section we study the problem of finding simple-loop gaits of maximal displacement as an optimal control problem. We begin by a review of Tam and Hosoi's method of representing the gait by a truncated Fourier series [25]. Then we transform the swimmer's shape variables into polar coordinates, formulate the optimal control problem, and derive its solution using Pontryagin's maximum principle. Most of this section considers the case where all links are equal $l_0 = l_1 = l_2$, where swimming distances are scaled by the swimmer's total length $l = l_0 + l_1 + l_2$. The last part of this section studies numerical optimization of the ratio of link's length for maximal net displacement.

### A. Review of Tam and Hosoi's optimization

Tam and Hosoi [25] represented gaits which are composed of time-periodic functions for the joint angles $\phi_1(t)$, $\phi_2(t)$ as truncated Fourier series. They considered only gaits that are symmetric with respect to the diagonal lines $\phi_1 = \phi_2$ and $\phi_1 = -\phi_2$, and used the alternative angles $\hat{\phi}_1$, $\hat{\phi}_1$, which are measured along axes that are aligned with the diagonal symmetry lines, see Fig. 1c. Using symmetries around the two diagonal axes, the gait can be represented by two Fourier series as:

$$\begin{aligned} \hat{\phi}_1(t) &= \sum_{k=1}^{N} a_k \cos((2k-1)t) \\ \hat{\phi}_2(t) &= \sum_{k=1}^{N} b_k \sin((2k-1)t) \end{aligned} \tag{9}$$

for $t \in [0, 2\pi]$. The infinite series is truncated at $k = N$, hence each gait is parametrized by the $2N$ scalar coefficients $\{a_i, b_i\}$. In order to find the optimal gait, we used MATLAB's function **fmincon**, for truncations of $N = \{1, 2, 3\}$. Trajectories of the optimal gaits are plotted in Fig. 2, where the displacement $X$ under each gait also appears on the plot (scaled by the swimmer's total length $l$). We also computed the optimal coefficients for $N = 4$, and the resulting trajectory is not visually distinguishable from that of $N = 3$, with less that $0.1\%$ increase in the displacement $X$.

### B. Symmetric gaits of simple loops in polar coordinates

We now introduce the transformation of shape variables $\phi_1, \phi_2$ into polar coordinates $r, \alpha$, as shown in Fig. 1b. The relation between the two sets of variables is given by

$$\begin{aligned} \phi_1 &= r \cdot \cos\alpha \\ \phi_2 &= r \cdot \sin\alpha \end{aligned} \tag{10}$$

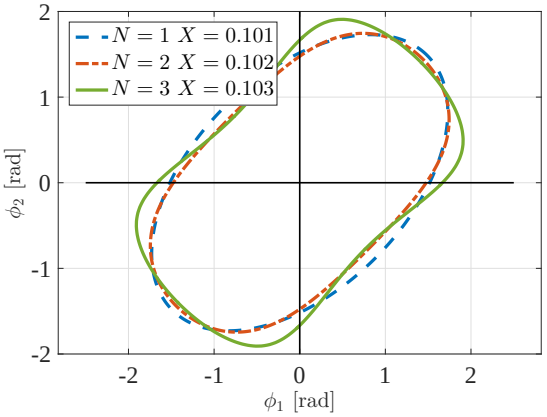


Fig. 2: Optimized gaits using $N$ Fourier coefficients, for $N = 1, 2, 3$.

By substituting (10) into (7), the swimmer's dynamics can now be written as:

$$\mathbf{V}_b = \mathbf{G}(r,\alpha)\mathbf{J}(r,\alpha)\begin{bmatrix} \dot{r} \\ \dot{\alpha} \end{bmatrix}, \tag{11}$$

where

$$\mathbf{J}(r,\alpha) = \begin{bmatrix} \cos\alpha & -r\cdot\sin\alpha \\ \sin\alpha & r\cdot\cos\alpha \end{bmatrix} \tag{12}$$

is the Jacobian matrix of the transformation in (10). The dynamic equations of $x(t)$ and $\theta(t)$ in (11) are written explicitly as:

$$\begin{aligned} \dot{x} &= g(r,\alpha,\theta)\dot{r} + h(r,\alpha,\theta)\dot{\alpha} \\ \dot{\theta} &= p(r,\alpha)\dot{r} + q(r,\alpha)\dot{\alpha} \end{aligned} \tag{13}$$

As explained in the previous section, the functions $p$ and $q$ associated with $\dot{\theta}$ in (13) are independent of $\theta$. Due to the time invariance property of the swimmer's dynamics, we can arbitrarily choose the time rate along the gait by setting $\dot{\alpha} = 1$, without affecting the net displacement $X$. Therefore, the gait is described by a single function $r(\alpha)$. Assuming a symmetric gait, we consider only one quarter of the trajectory with $\alpha \in [\frac{\pi}{4}, \frac{3\pi}{4}]$, and the resulting net displacement is multiplied by four to obtain $X$. Thus, we set

$$\alpha = t + \frac{\pi}{4} \text{ for } t \in [0, t_f], \tag{14}$$

where the final time is $t_f = \frac{\pi}{2}$.

### C. Formulating the optimal control problem

We now formulate the optimal control problem for maximizing the net displacement of Purcell's swimmer. Let $\mathbf{z}(t)$ be the state vector

$$\mathbf{z} = \begin{bmatrix} r \\ \theta \end{bmatrix} \tag{15}$$

The polar angle $\alpha$ is not included in $\mathbf{z}$ since it is an independent variable which is related to time via (14). The control input of the system is defined as $u(t) = dr/dt = dr/d\alpha$. The control system is thus given by

$$\dot{\mathbf{z}}(t) = \begin{bmatrix} u(t) \\ p(r,\alpha(t))u(t) + q(r,\alpha(t)) \end{bmatrix}. \tag{16}$$

The initial rotation is chosen as $\theta(0) = 0$, while $r(0)$ is unspecified. The end conditions $r(t_f)$ and $\theta(t_f)$ are also unspecified. We wish to maximize the displacement in $x$ direction. Using equation (13), the cost function is given by the integral:

$$J = x(t_f) = \int_0^{t_f} g(r,\theta,t)u + h(r,\theta,t)dt. \tag{17}$$

The optimal control problem is finding the control $u(t)$ which maximizes the cost function $J = x(t_f)$. The solution is obtained by using the formulation of Pontryagin's maximum principle [29], [30], [31], as follows. The costate vector is defined as $\boldsymbol{\lambda} = [\lambda_1(t), \lambda_2(t)]^T$, and the Hamiltonian $H$ is given by

$$H(\mathbf{z}, u, \boldsymbol{\lambda}) = gu + h + \lambda_1 u + \lambda_2(pu + q). \tag{18}$$

The costate equations are:

$$\begin{aligned} \dot{\lambda}_1 &= -\frac{\partial H}{\partial r} = -g_r u - h_r - \lambda_2 p_r u - \lambda_2 q_r, \\ \dot{\lambda}_2 &= -\frac{\partial H}{\partial \theta} = -g_\theta u - h_\theta, \end{aligned} \tag{19}$$

where subscripts denote partial derivatives, for example: $g_r = \frac{\partial g}{\partial r}$. Transversality conditions for unspecified boundary conditions of $\mathbf{z}(t)$ imply that $\lambda_1(t_f) = \lambda_2(t_f) = \lambda_1(0) = 0$. Pontryagin's maximum principle states that an optimal control $u^*(t)$ must satisfy

$$\frac{\partial H\left(\mathbf{x}(t), u(t), \boldsymbol{\lambda}(t)\right)}{\partial u} = 0. \tag{20}$$

However, (18) implies that the Hamiltonian is linear in $u$, and thus the control input does not appear in the derivative, which is given by:

$$\frac{\partial H}{\partial u} = H_u(\mathbf{z}(t), u(t), \boldsymbol{\lambda}(t)) = g + \lambda_1 + \lambda_2 p. \tag{21}$$

In cases where the control is bounded, this implies a "bang-bang" solution where $u(t)$ lies on boundaries of its permissible range, as proposed in the analysis of [38]. Since there are no physical bounds on $u(t)$ here, the optimal solution must follow a *singular arc*, where $H_u(t)$ vanishes identically [29], [30]. Thus, the optimal control $u^*(t)$ should be obtained by requiring that the time derivatives of $H_u$ vanish as well:

$$\dot{H}_u(t) = 0, \quad \ddot{H}_u(t) = 0 \quad \forall t. \tag{22}$$

Applying the chain rule to (21) and substituting the derivatives from (16) and (19), The first-order time derivative is:

$$\dot{H}_u = \lambda_2(p_\alpha - q_r) + g_\theta q + g_\alpha - h_\theta p - h_r = 0. \tag{23}$$

As expected [29], [30], the control does not appear in (23), but only in the second-order derivative, which is obtained as

$$\ddot{H}_u = D(\mathbf{z}, \lambda_2, t)u(t) + N(\mathbf{z}, \lambda_2, t) = 0, \tag{24}$$

where

$$\begin{aligned} D(\mathbf{z},\lambda_2,\alpha) = \; & g_{r\alpha} - h_{rr} - h_{r\theta}p + g_{\theta\alpha}p + g_\theta q_r + h_\theta p_r - g_\theta(p_\alpha - q_r) \\ & + \lambda_2(p_{r\alpha} - q_{rr}) + q(g_{r\theta} + g_{\theta\theta}p) - p(h_{r\theta} + h_{\theta\theta}p) \end{aligned} \tag{25}$$

and

$$\begin{aligned} N(\mathbf{z},\lambda_2,t) = \; & g_{\alpha\alpha} - h_{r\alpha} - h_{r\theta}q + g_{\theta\alpha}q + g_\theta q_\alpha + h_\theta p_\alpha - h_\theta(p_\alpha - q_r) \\ & + \lambda_2(p_{\alpha\alpha} - q_{r\alpha}) + q(g_{\theta\alpha} + g_{\theta\theta}q) - p(h_{\theta\alpha} + h_{\theta\theta}q). \end{aligned} \tag{26}$$

Second-order derivatives are denoted by two subscripts in (25),(26), for example, $g_{r\theta} = \frac{\partial^2 g}{\partial r \partial \theta}$. The optimal control input is therefore obtained by requiring $\ddot{H}_u(t) = 0$ as:

$$u^* = u^*(\mathbf{z}, \lambda_2, t) = -\frac{N(\mathbf{z}, \lambda_2, t)}{D(\mathbf{z}, \lambda_2, t)}. \tag{27}$$

The derivatives in (19) and (27) can be obtained explicitly from (7) and (13) by applying the chain rule on the transformation (10). Note that the costate equations in (19) as well as the optimal control $u^*$ in (27) are all independent of $\lambda_1$, and thus, one has to solve only a system of three equations in $\{r(t), \theta(t), \lambda_2(t)\}$. However, after reducing $\lambda_1$, two boundary condition were eliminated. The missing boundary

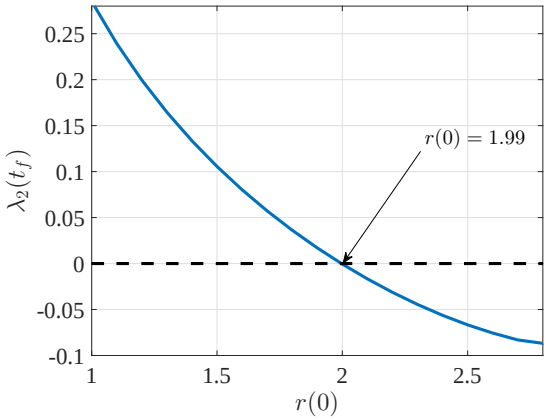


Fig. 3: $\lambda_2(t_f)$ as a function of the guessed value of $r(0)$.

condition can be obtained from the requirement that $\dot{H}_u(t = 0) = 0$. Using (23) then gives a relation between $\lambda_2(0)$ and $r(0)$, which, together with $\theta(0) = \lambda_2(t_f) = 0$, complete the three required boundary conditions of the reduced system.

### D. Computing the optimal solution

The boundary value problem is solved by using simple one-dimensional shooting, explained as follows. First, we guess an initial condition for $r(0)$. Then, we use $\dot{H}_u(0) = 0$ from (23) in order to obtain $\lambda_2(0)$. Using the three initial conditions, the nonlinear system in $\{r(t), \theta(t), \lambda_2(t)\}$ is solved using MATLAB's **ode45** command, and the terminal value $\lambda_2(t_f)$ is computed. Repeating the process while varying the guess of $r(0)$, Fig. 3 plots $\lambda_2(t_f)$ as a function of the guess $r(0)$. The correct guess of $r(0) = 1.99$ which results in $\lambda_2(t_f) = 0$ is easily obtained via bisection, and the full system of state and costate equations (16),(19) under the optimal input $u^*$ in (27) is integrated numerically. Plots of the optimal solution of $r^*(t)$ and $\theta^*(t)$ are shown in Figs. 4a and 4b, respectively. Solution of the costates $\lambda_i(t)$ is plotted in Fig. 4c, and the optimal input $u^*(t)$ is plotted in Fig. 4d. Relation (14) can now be used in order to obtain the polar description of the quarter gait $r^*(\alpha)$. Completing to a full period using symmetry reflections and applying the transformation (10), the gait trajectory in $(\phi_1, \phi_2)$ plane is then obtained. It is exactly identical (not visually distinguishable) to Tam and Hosoi's gait in Fig. 1c, and to the gait obtained using optimized Fourier coefficients with $N = 3$ in Fig. 2, where the maximal numerical deviation in $r(\alpha)$ is less than $0.01$ radians. From Figs. 4a and 4d, one can observe that the optimal solution satisfies $\dot{r}^*(0) = \dot{r}^*(t_f) = 0$. This implies that on the diagonal axes of symmetry, reflected curves of quarter gaits are connected tangentially and form a full closed loop which is a smooth curve, as expected. Additionally, Fig. 4b indicates that the swimmer undergoes a considerable amount of rotation during the optimal motion, with peaks of $0.56$ radians (approx $32°$). Finally, [29], [30] mention that in order to check that the solution through a singular arc (with $\ddot{H}_u(t) = 0$) actually attains a local maximum, an additional necessary condition is given by

$$\frac{\partial \ddot{H}_u}{\partial u}(t) \geq 0 \ \ \forall t. \tag{28}$$

It can be shown that in our case, this condition is equivalent to $D(t) > 0$ where $D$ is defined in (25). The plot of $D(t)$ is shown in dashed curve in Fig. 4d, which indicates that this condition is indeed satisfied.

## IV. CONCLUSION

In this work, we have studied displacement-optimal gaits of Purcell's three-link swimmer using optimal control approach. We used polar coordinates representation of a symmetric simple loop and analytically formulated an optimal control problem with two state variables and a single input. Due to absence of physical constraints on the system's input, Pontryagin's principle implied that the optimal solution must follow a singular arc. The resulting boundary value problem has been solved numerically, and the optimal solution exactly reproduced the optimal gait of Tam and Hosoi [25]. Finally, we have numerically obtained the optimal ratio of the swimmer's links lengths that achieves maximal displacement.

We now briefly discuss limitations of the results and list several directions for possible future extensions. First, we are currently working on experimental realization of the results on a macro-scale robotic swimmer in a highly viscous silicone fluid. A previous tethered prototype has been used in [21], which had mechanical limitations on the joint angles that precluded application of large-amplitude gaits. A new untethered prototype that enables large strokes has recently been constructed, which will hopefully enable demonstration of the optimal gait. Second, explicit formulation of Purcell's swimmer dynamics has been conducted here under the simplifying RFT paradigm of local drag resistance, that

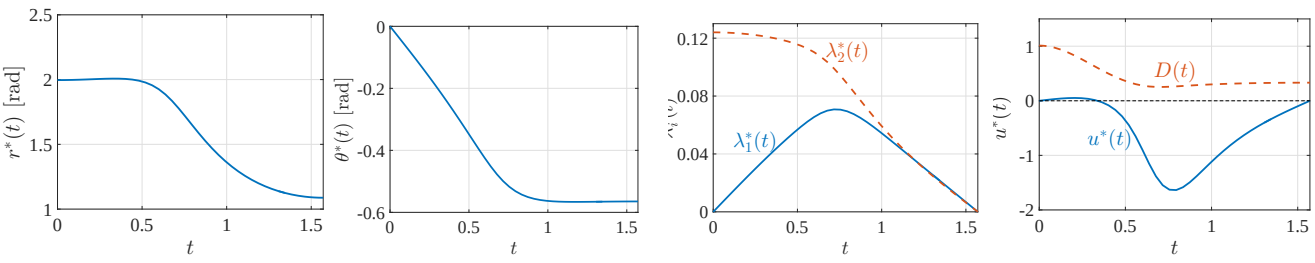


(a) (b) (c) (d)

Fig. 4: Plots of the optimal solution: (a) $r^*(t)$, (b) $\theta^*(t)$, (c) costates $\lambda_i^*(t)$, and (d) optimal control input $u^*(t)$.

is, hydrodynamic interaction between the links has been neglected. In principle, our method can also work with more accurate formulations that account for finite slenderness of the links as in [23] and [25], where the governing dynamic equations in (7) and (13) can be obtained only numerically. In this case, all partial derivatives in the optimal control system (19), (25) and (25) should be numerically approximated using finite-differences of any desired order. (We have tried this numerical approach for our RFT formulation and obtained exactly the same optimal gait). Moreover, the same method can also be applied to obtain optimal gaits for an inertia-dominated large three-link swimmer in an "insviscid fluid" as in [14], [15]. Finally, it is planned to extend the results presented here and attempt to utilize optimal control techniques for several models of microswimmers in which the dynamics is time-dependent, such as Purcell's swimmer with a passive elastic joint [41] and the magnetically-actuated multi-link microswimmers [42], [43], [44].

## REFERENCES


[1] E. Lauga and T. R. Powers, "The hydrodynamics of swimming microorganisms," *Reports on Progress in Physics*, vol. 72, no. 9, p. 096601, 2009.

[2] E. Lauga, "Bacterial hydrodynamics," *Annu. Rev. Fluid Mech. (in press, arXiv preprint arXiv:1509.02184)*, 2016.

[3] R. Dreyfus, J. Baudry, M. L. Roper, M. Fermigier, H. A. Stone, and J. Bibette, "Microscopic artificial swimmers," *Nature*, vol. 437, pp. 862–865, 2005.

[4] J. J. Abbott, M. C. Lagomarsino, L. Zhang, L. Dong, and B. J. Nelson, "How should microrobots swim?" *The International Journal of Robotics Research*, 2009.

[5] W. Gao, D. Kagan, O. S. Pak, C. Clawson, S. Campuzano, E. Chuluun-Erdene, E. Shipton, E. E. Fullerton, L. Zhang, E. Lauga, and J. Wang, "Cargo-towing fuel-free magnetic nanoswimmers for targeted drug delivery," *small*, vol. 8, no. 3, pp. 460–467, 2012.

[6] M. Sitti, H. Ceylan, W. Hu, J. Giltinan, M. Turan, S. Yim, and E. Diller, "Biomedical applications of untethered mobile milli/microrobots," *Proceedings of the IEEE*, vol. 103, no. 2, pp. 205–224, 2015.

[7] G. Kósa, P. Jakab, N. Hata, F. Jólesz, Z. Neubach, M. Shoham, M. Zaaroor, and G. Székely, "Flagellar swimming for medical micro robots: theory, experiments and application," in *2nd IEEE RAS & EMBS International Conference on Biomedical Robotics and Biomechatronics (BioRob)*, 2008, pp. 258–263.

[8] J. Koiller, R. Montgomery, and K. Ehlers, "Problems and progress in microswimming," *J. Nonlinear Science*, vol. 6, pp. 507–541, 1996.

[9] J. S. Martin, T. Takahashi, and M. Tucsnak, "A control theoretic approach to the swimming of microscopic organisms," *Quarterly of Applied Mathematics*, vol. 65, no. 3, pp. 405–424, 2007.

[10] F. Bullo and A. D. Lewis, *Geometric Control of Mechanical Systems*. New York: Springer, 2005.

[11] J. Lohéac, J.-F. Scheid, and M. Tucsnak, "Controllability and time optimal control for low Reynolds numbers swimmers," *Acta Applicandae Mathematicae*, vol. 123, no. 1, pp. 175–200, 2013.

[12] S. D. Kelly and R. M. Murray, "Geometric phases and robotic locomotion," *J. of Robotic Systems*, vol. 12, no. 6, pp. 417–431, 1995.

[13] J. Ostrowski and J. Burdick, "The geometric mechanics of undulatory robotic locomotion," *International Journal of Robotics Research*, vol. 17, no. 7, pp. 683–701, 1998.

[14] E. Kanso, J. E. Marsden, C. W. Rowley, and J. B. Melli-Huber, "Locomotion of articulated bodies in a perfect fluid," *J. Nonlinear Sci.*, vol. 15, no. 4, pp. 255–289, 2005.

[15] R. L. Hatton, Y. Ding, H. Choset, and D. I. Goldman, "Geometric visualization of self-propulsion in a complex medium," *Physical Review Letters*, vol. 110, no. 7, p. 078101, 2013.

[16] E. M. Purcell, "Life at low Reynolds number," *Am. J. Phys*, vol. 45, no. 1, pp. 3–11, 1977.

[17] L. E. Becker, S. A. Koehler, and H. A. Stone, "On self-propulsion of micro-machines at low Reynolds number: Purcell's three-link swimmer," *Journal of Fluid Mechanics*, vol. 490, pp. 15–35, 2003.

[18] J. Gray and G. Hancock, "The propulsion of sea-urchin spermatozoa," *Journal of Experimental Biology*, vol. 32, no. 4, pp. 802–814, 1955.

[19] R. G. Cox, "The motion of long slender bodies in a viscous fluid part 1. general theory," *J. Fluid Mech.*, vol. 44, pp. 791–810, 1970.

[20] J. E. Avron and O. Raz, "A geometric theory of swimming: Purcell's swimmer and its symmetrized cousin," *New J. Phys.*, vol. 10, p. 063016, 2008.

[21] E. Gutman and Y. Or, "Symmetries and gaits for Purcell's three-link microswimmer model," *IEEE Trans. Robotics*, vol. 32, no. 1, pp. 53–69, 2016.

[22] M. S. Kumar and P. Philominathan, "Robo-linked Purcell's swimmer," *International Journal of Fluid Mechanics Research*, vol. 38, no. 6, 2011.

[23] G. Huber, S. A. Koehler, and J. Yang, "Micro-swimmers with hydrodynamic interactions," *Mathematical and Computer Modelling*, vol. 53, no. 7, pp. 1518–1526, 2011.

[24] O. Wiezel and Y. Or, "Optimization and small-amplitude analysis of Purcell's three-link microswimmer model," *Proc. Roy. Soc. A, to appear.* Preprint at ArXiv, http://arxiv.org/abs/1603.02268.

[25] D. Tam and A. E. Hosoi, "Optimal stroke patterns for Purcell's three-link swimmer," *Physical Review Letters*, vol. 98, p. 068105, 2007.

[26] A. Shapere and F. Wilczek, "Efficiencies of self-propulsion at low Reynolds number," *Journal of Fluid Mechanics*, vol. 198, pp. 587–599, 1989.

[27] J. E. Avron, O. Gat, and O. Kenneth, "Optimal swimming at low Reynolds numbers," *Phys Rev. Lett.*, vol. 93, no. 18, p. 186001, 2004.

[28] S. E. Spagnolie and E. Lauga, "The optimal elastic flagellum," *Physics of Fluids (1994-present)*, vol. 22, no. 3, p. 031901, 2010.

[29] A. Bryson and Y.-C. Ho, "Applied optimal control" *CRC Press*, 1975.

[30] J. Z. Ben-Asher, *Optimal control theory with aerospace applications*. American Institute of Aeronautics and Astronautics, 2010.

[31] L. S. Pontryagin, *Mathematical theory of optimal processes (English translation)*. CRC Press, 1987.

[32] J. P. Ostrowski, J. P. Desai, and V. Kumar, "Optimal gait selection for nonholonomic locomotion systems," *The International Journal of Robotics Research*, vol. 19, no. 3, pp. 225–237, 2000.

[33] E. Kanso and J. E. Marsden, "Optimal motion of an articulated body in a perfect fluid," in *Proc. IEEE Conf. on Decision and Control*, 2005, pp. 2511–2516.

[34] S. Ober-Blöbaum, O. Junge, and J. E. Marsden, "Discrete mechanics and optimal control: an analysis," *ESAIM: Control, Optimisation and Calculus of Variations*, vol. 17, no. 02, pp. 322–352, 2011.

[35] M. B. Kobilarov and J. E. Marsden, "Discrete geometric optimal control on lie groups," *IEEE Transactions on Robotics*, vol. 27, no. 4, pp. 641–655, 2011.

[36] F. Alouges, A. DeSimone, and A. Lefebvre, "Optimal strokes for axisymmetric microswimmers," *The European Physical Journal E: Soft Matter and Biological Physics*, vol. 28, no. 3, pp. 279–284, 2009.

[37] L. Giraldi, P. Martinon, and M. Zoppello, "Controllability and optimal strokes for N-link microswimmer," in *Proc. IEEE Conf. on Decision and Control*, 2013, pp. 3870–3875.

[38] L. Giraldi, P. Martinon, and M. Zoppello., "Optimal design of the three-link Purcell swimmer," *Physical Review E*, vol. 91, p. 023012, 2015.

[39] O. Raz and J. E. Avron, "Comment on 'optimal stroke patterns for Purcell's three-link swimmer'," *Physical Review Letters*, vol. 100, p. 029801, Jan 2008. [Online]. Available: http://link.aps.org/doi/10.1103/PhysRevLett.100.029801

[40] J. Happel and H. Brenner, *Low Reynolds Number Hydrodynamics*. Prentice-Hall, 1965.

[41] E. Passov (Gutman) and Y. Or, "Dynamics of Purcell's three-link microswimmer with a passive elastic tail," *The European Physical Journal E*, vol. 35, no. 8, pp. 1–9, 2012.

[42] E. Gutman and Y. Or, "Simple model of a planar undulating magnetic microswimmer," *Physical Review E*, vol. 90, no. 1, p. 013012, 2014.

[43] B. Jang, E. Gutman, N. Stucki, B. F. Seitz, P. D. Wendel-García, T. Newton, J. Pokki, O. Ergeneman, S. Pané, Y. Or and B. J. Nelson, "Undulatory locomotion of magnetic multilink nanoswimmers," *Nano letters*, vol. 15, no. 7, pp. 4829–4833, 2015.

[44] F. Alouges, A. DeSimone, L. Giraldi, and M. Zoppello, "Can magnetic multilayers propel artificial microswimmers mimicking sperm cells?" *Soft Robotics*, vol. 2, no. 3, pp. 117–128, 2015.